Available online at www.sciencedirect.com
SCIENCE DIRECT®
Journal of Nuclear Materials 336 (2005) 125–134
journal of nuclear materials
www.elsevier.com/locate/jnucmat

A model study of displacement cascades distributions in zirconium

M. Hou [a,*], D. Kulikov [a,b]

[a] *Physique des Solides Irradiés et des Nanostructures CP234, Université Libre de Bruxelles, Boulevard du Triomphe, B-1050 Bruxelles, Belgium*
[b] *A.F. Ioffe Physico-Technical Institute of RAS, Polytechnicheskaya Str. 26, 194021 St. Petersburg, Russia*

Received 8 June 2004; accepted 17 September 2004

Abstract

5 to 200 keV displacement cascades in zirconium are studied in the binary collision approximation with the simulation code Marlowe. The cascades are analysed statistically by means of component analysis, fuzzy clustering and isodata analysis. As a consequence of the large recoil ranges and range straggling specific to open hcp lattices like Zr, a large dispersion of the frequencies of Frenkel pair distributions is found, as well as of the spatial extent and morphology of vacancy and interstitial distributions. In Zr, cascades are formed by a widespread distribution of displacement clusters that can be small. Remarkably, the size and morphology distributions of these clusters are found independent of the primary recoil energy in the energy range investigated.

1. Introduction

Zirconium-based materials are used in nuclear technology because of their resistance to neutron irradiation. However, radiation damage accumulates on the long term and hampers mechanical properties and resistance against corrosion. This problem motivates substantial effort in order to understand damage evolution in radiation environment. For understanding, model systems are considered and a significant amount of comprehensive experimental studies is available [1]. With experimental techniques, macroscopic and mesoscopic properties and their modifications can be identified. However, radiation damage initiates from the interaction of neutrons with atoms and develops at the atomic scale. This leads to a major difficulty since the information which can be gathered experimentally at the atomic scale is limited. For this reason, atomic scale and multiscale computer modelling are developed with the hope to bridge the gap between the initial damaging processes and the macroscopic material modifications. The SIRENA project [2] is one initiative in this direction and the present work enters in this context. This study aims at understanding the first steps of damage evolution as a consequence of a collision between a neutron and an atom in the Zr lattice. Such a collision results in the knock-off of an energetic Zr atom and the primary energies considered here range from 5 to 200 keV. The primary knock-on atom (PKA) looses its energy via electronic excitation and by generating a cascade of secondary knock-on atoms. This cascade is responsible for more than 90% of the

* Corresponding author. Tel.: +32 2 650 5735; fax: +32 2 650 5227.
E-mail address: mhou@ulb.ac.be (M. Hou).

0022-3115/$ - see front matter
doi:10.1016/j.jnucmat.2004.09.013

energy dissipation which results in a series of stable vacancies and interstitials. These represent the primary damage. Its generation does not require more than 1 ps and its frequency and spatial distributions are characterised below. Point defects and particularly interstitials, are mobile. Since typical temperatures in radiation environment are of the order of several hundred Kelvin, thermal diffusion is activated and cascade point defects regroup to form complexes [3,4]. The characteristic time for their formation is less than 1 ns. This represents the defect evolution stage next to the generation of point defects. In a third stage, these complexes may grow because of further primary damage generation in the environment and give rise to still larger defects, as dislocation loops, that can be observed experimentally.

The natural modelling technique for predicting atomic-scale damage generation is molecular dynamics (MD) and it is nowadays realistic to follow the evolution of a collection of collision cascades over 1 ns, hence, until the recombination of vacancies and interstitials into complexes. Previous cascade studies in cubic materials demonstrate a large dispersion of point defect cascade properties, making it necessary to generate samples of tens of thousands of events for characterizing their properties correctly. This is not feasible by full MD, but this objective can be reached within limited computer effort by using the binary collision approximation (BCA) of MD. This approximation is well-known and will not be presented here in detail. It is described in detail, for instance, in [5]. Many comparisons between BCA and full MD are available, for instance, in [6–10].

In the next section, the essential features of the BCA model are given and the parameterization of BCA on MD is discussed, leading to a comprehensive prediction of the number of Frenkel pairs on the damage energy. Section 3 describes the tools used to analyse vacancy and interstitial distributions, and the properties of these distributions are emphasised in Section 4. The picture emerging from this analysis is summarised in Section 5.

2. Parameterisation of the binary collision approximation

In the binary collision approximation as used in the Marlowe program [11], collision cascades are modelled as sequences of binary encounters. For trajectory calculation, we use the Molière approximation to the Thomas–Fermi potential [12] with the expression of the screening length suggested by Firsov [13]. The binary collisions are ordered in time, so as to respect the chronological development of the cascades. Lattice atoms are considered as bound to their equilibrium position with a binding energy equal to the cohesive energy of Zr. The sequence of collisions undergone by each atom in the cascades is calculated until its kinetic energy falls below the value of the cohesive energy. For the purpose of comparison with MD, electronic energy losses along the trajectories are neglected and, as a consequence, the PKA energy is entirely available for damage. At the end of each cascade, vacancies and interstitials are assumed to recombine thermally if their separation distance is smaller than some recombination distance used as a parameter. A Frenkel pair is thus assumed to be stable only if the distance between the vacancy and the interstitial exceeds a threshold recombination distance, r_c. If the separation is smaller than r_c then a Frenkel pair is considered to recombine athermally. Using this model, it was found in a previous work, in the case of copper and gold [7], that the time dependence of the number of moving cascade atoms with total energy above a given value is in good agreement with full MD as long as this given value is positive. When the total energy is negative, a purely repulsive potential as used here is unsuitable. This recombination distance can be adjusted by matching the number of stable Frenkel pairs produced for the prediction of full MD. The procedure was already successfully applied to cascades in iron for a PKA energy range between 5 and 20 keV [8]. Adjusting r_c in such a way as to match the number of Frenkel pairs predicted in the BCA to the MD prediction for a given PKA energy, good matching was found over the whole range of energies considered and the number of Frenkel pairs produced is not significantly dependent on the potential used. More MD results, covering a larger energy range, are presently available. Since full MD estimates of the number of Frenkel pairs in Zr are not quite numerous, it is worth briefly revisiting the problem of such a parameterization in the case of Fe prior to the case of Zr. In Fig. 1, we show a comparison for Fe using a number of MD data known from literature [8,14–16]. According to [14] we can find an approximation of the dependence of the number Frenkel pairs, N_F, on the PKA energy, E, as $N_F = A*E^m$, where E is expressed in keV. In Table 1,

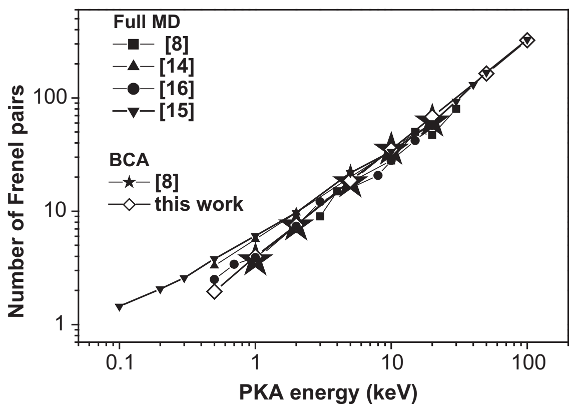

Fig. 1. Mean number of Frenkel pairs vs. the initial PKA energy as obtained for iron by MD and BCA at 100 K.

Table 1
Exponents m in the dependence of the number of Frenkel pairs, N_F, on PKA energy, E, ($N_F = A*E^m$) as obtained by fitting different molecular dynamics (MD) and binary collision approximation (BCA) results for iron

$E < 1$ keV	$1 < E < 10$ keV	$E > 10$ keV	References
	0.78		MD, [14]
0.485	0.795	1.12	MD, [15]
	0.87		MD, [8]
0.62	0.79	1.08	MD, [16]
	0.945		BCA, [8], (AMLJ potential)
	0.957		BCA, present work, (Molière potential)

In the BCA, results obtained with the average modified Lens-Jensens (AMLJ) potential are given.

the exponent m in this expression is given for the different MD and BCA results presented in Fig. 1. The dependences obtained with the BCA have the same exponent in the whole energy range from 0.1 to 100 keV whereas the MD dependence has no constant slope. Hence, the MD exponents vary with PKA energy. BCA results in the present work and in [8] were obtained with different potentials and therefore different values of the recombination radius r_c were used. The exponent m is not found significantly dependent on the recombination radius, nor on the potential. In Fig. 1 and Table 1 it is seen that the agreement between MD and BCA is the best at high energies. Here, the Molière potential was used, with $r_c = 4.75$ lattice units. The value of the exponent $m = 1$ is consistent with the ballistic theory of Kinchin and Pease [17] and, subsequently, with the so-called NRT model [18]. The exponent $m < 1$ is determined empirically and no physical interpretation is suggested nowadays. The coincidence of the BCA and MD for m tending to 1 at high PKA energy indicates the ballistic character of the collision cascades while the origin of the offset at low PKA energy obtained by MD is still the purpose of on-going studies.

The same analysis is now repeated for the case of zirconium. We use the MD results in [14,19] for adjusting the recombination radius at 10 keV PKA energy. The matching value of r_c is 5 lattice units and this value is not significantly temperature dependent. The comparison is possible in the energy range from 0.5 to 20 keV in which MD data are available and the results are shown in Fig. 2 for energies between 0.5 and 200 keV. In this energy range, like for Fe, it is seen that the exponent of the power law is lower in the case of MD than predicted in the BCA. The exponent in the BCA results is again close to unity and is not significantly dependent on the recombination distance used. It is also found independent of the value of the screening distance in the Molière potential. Anyway, the comparison shows that, within the energy range from 5 to 20 keV and with such a recombination radius, the quantitative agreement between MD and the BCA is excellent. It is still reasonable both at lower and at higher energies. This incites using the BCA with good statistics for collision cascade calculations at high energies instead of MD calculations that would be prohibitively long. The statistical analysis of the results in Fig. 2 reveals a very significant difference between the cases of Zr and Fe. In the latter, both in MD and BCA predictions, the standard deviation of the frequency distribution of the number of Frenkel pairs are a few percent [8,20,21], even at high energy, consistent with the early analytical theory for structureless materials [22]. The standard deviation of the Frenkel pair frequency distributions is not larger than the size of the points represented in Fig. 1 (no more than 5% of the mean). They are represented in Fig. 2 in the case of Zr, which has an hcp structure. The standard deviation is 20% of the mean at 5 keV energy. It increases with energy and is found as high as 50% of the mean at 25 keV and 85% of the mean at 200 keV. Hence, the dispersion which is huge as compared to other BCA results,

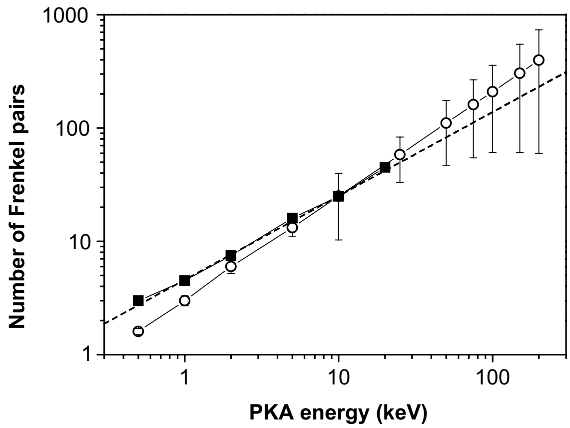

Fig. 2. Mean number of Frenkel pairs vs. initial PKA energy as obtained by MD and BCA for cascades in Zr at 100 K. Squares: MD results in [14,19]; dashed line: fitting equation of the for MD results ($m = 0.74$); circles: BCA results; solid line: fitting equation for BCA results ($m = 0.925$). The recombination distance is matched at 10 keV. Standard deviations of the BCA frequency distributions are shown by vertical bars. Standard errors on BCA results are smaller than the size of the points.

increases with the PKA energy. It is worth mentioning here that, although the dispersion is large, by accumulating statistics over 5000 cascades at each energy, the standard error on the mean in Fig. 2 is no more than 1% at 200 keV. The origin of such broad frequency distributions is identified to originate from two factors: one is the lower density of Zr and the second is the hcp structure which is more open in several directions than cubic structures and equally compact in others. It was possible to reach this conclusion by running BCA simulations with artificial crystals. Since the BCA does not require the system to be at mechanical equilibrium, it is possible to modify one single parameter keeping all others constant. The first parameter changed was the mass of Zr in order to check for an isotopic effect. The primary energy was 25 keV. It was found that doubling the mass of Zr brings no modification in the Frenkel pair distance distribution nor to the standard deviation of the frequency distributions for each Frenkel pair separation distance. These frequencies remain about 50% of the mean, whatever the separation distances. This large dispersion is a lattice effect which can be illustrated by primary recoil range distributions. Mean primary recoil ranges are shown in Fig. 3(a) and ranges straggling in Fig. 3(b). Like for calculating cascades, primaries are initiated at a lattice site and their initial directions are selected isotropically and at random. Primary trajectories are followed until their kinetic energy falls below a cutoff value equal to the cohesive energy of Zr. The range is the measure of the distance between the end point and the initial location of the primary. The straggling is the standard deviation of the range distribution. Both mean PKA ranges and straggling are found to be fast increasing functions of the initial energy. The straggling reaches 100% of the mean at 200 keV which is to be compared with the 85% standard deviation of the Frenkel pair frequency distribution in Fig. 2. It is straightforward in a BCA code to model an amorphous solid. In Marlowe, an amorphous structure is modelled by a random rotation of the lattice structure before each collision. This procedure preserves the density of the crystalline material as well as the first neighbour distances and it destroys directional correlations. Using this model, primary recoil calculations were repeated, keeping all other model parameters constant. The reduction of the range and straggling, as compared to the case of a single crystal, is drastic. This demonstrates the strong directional effect on recoil ranges in crystalline Zr. The fact that the dispersion of recoil ranges is large reveals that the dispersion of specific energy loss by primaries is large too, hence the number of secondary recoils and, subsequently, the number of Frenkel pairs. The qualitative difference between the dispersion of BCA results in Figs. 1 and 2 can be explained as well. This can be done by repeating the range calculations again, assigning an artificial bcc structure to the lattice and adjusting the lattice

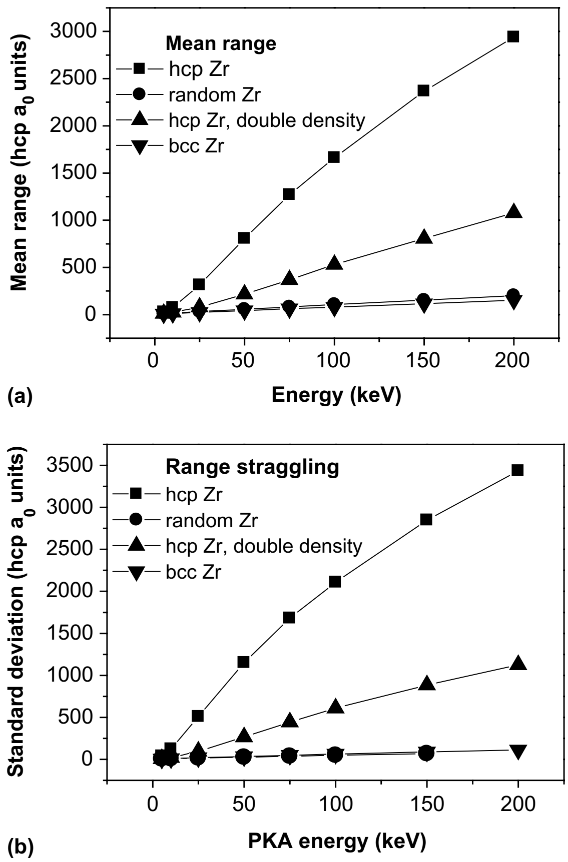

Fig. 3. Mean ranges (a) and ranges straggling (b) for different Zr model structures, as predicted in the BCA.

distance in such a way that the density is the same as the hcp. As seen in Fig. 3, mean ranges and range straggling are found to be similar to the case of amorphous Zr. First neighbour distances in the bcc and the hcp lattices are comparable. The difference found in range distributions thus reflects the important role of the lattice anisotropy, which is more pronounced in hexagonal than in cubic lattices. It should be noticed that lattice anisotropy is not the only factor determining the range distributions. For instance, as already known from the range theory for structureless materials [23], they are also dependent on the material density. This is illustrated in Fig. 3 for hcp Zr by repeating the range calculations again, in a hypothetical Zr structure having the same *c*/*a* ratio as the real one but twice its density. Both the ranges and the straggling are significantly decreased, about a factor 2, but the effect is not as strong as the effect of the lattice anisotropy.

The characteristics of PKA range distributions discussed here have consequences not only on the number, but also on the spatial distributions of point defects. We thus present below a study of vacancy and interstitial distributions similar to that presented for iron in [8]. However, displacement cascades in Zr differ substantially from cascades in Fe and additional analysis tools are necessary. We use a fuzzy clustering method [24] completed by an Isodata analysis [25,26]. Although the detail of the method is presented in [27], it may be useful to summarize the basis, prior to the analysis. This is done in the next section.

3. Component analysis, fuzzy clustering and isodata

3.1. Component analysis

Displacement cascades are formed by vacancies and interstitials having, usually, different spatial extents. Their overall spatial distribution may conveniently be characterised by an ellipsoid of which axes directions and lengths are determined by component analysis (CA) [28]. We used CA extensively in previous studies of displacement cascades, generated in the BCA as well as by full MD, in iron. The directions of the axes are those of the eigenvectors of the covariance matrix of the spatial distribution. The associated eigenvalues, labelled α^2, β^2 and γ^2 in what follows are proportional to the variance of the spatial distribution projected onto the eigenvectors. The vectors parallel to the eigenvectors with lengths α, β and γ, and origin at the mean position of the distribution are the components. These vectors subtend the ellipsoid mentioned above which is taken as representative of the cascade volume and morphology. However, cascades may be complex objects and their representation by a single ellipsoid may not be sufficient, as is the case for Zr. Cascades may be formed by more than one convex cloud of point defects (vacancies or interstitials) and these may be connected by pipes, they may overlap or they may be well separated. This complexity is illustrated in Fig. 4 showing vacancies and interstitials generated by one 100 keV PKA. A visual inspection is not sufficient to surely distinguish subcascades, their overlaps and pipes, nor to decide which point defect belongs to which subcascade since their boundaries are fuzzy. It was therefore suggested in [27] to consider them as such and to apply the concepts of the theory of fuzzy sets to their analysis.

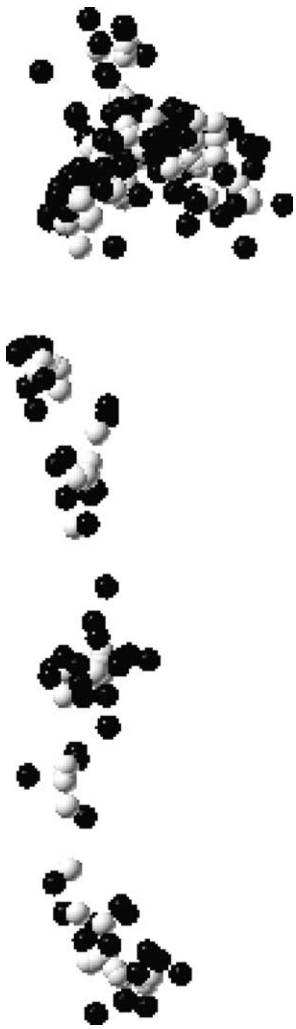

Fig. 4. One model cascade generated by a 100 keV primary knock-on atom. Vacancies are represented by light spheres and interstitials by dark spheres.

3.2. Fuzzy clustering

The theory of fuzzy sets, initiated by Zadeh [24], is merely a generalisation of the theory of conventional sets. A conventional set, with centre C, has well-defined boundaries and is defined by a characteristic function

$$\chi(K_C) = 1 \quad \text{if } x \in K_C \quad \text{and} \quad 0 \text{ otherwise.} \tag{1}$$

In the theory of fuzzy sets, this characteristic function is replaced by a 'grade of membership' or 'membership function', $\chi(K_C)$, of an object to a cluster K_C. The function χ (K_C) is a function defined between 0 and 1. For the analysis of cascades, we use a class of membership functions that can be expressed as

$$\chi(K_C) = f[\eta(x, C)]. \tag{2}$$

Here, $\chi(K_C) = 0$ if x does not belong to K_C and $\chi(K_C) = 1$ for the object x which belongs 'the most' to K_C. The grade of membership is a monotonic function of a distance $\eta(x, x^*)$ between an object x and a prototype x^* defined as the object C in K_C such that $\chi(K_C) = 1$. This way, it is admitted that an object may have a fractional non-zero grade of membership to different sets. Fuzzy clustering appears as a way of measuring the distance between an object and a prototype. If there are several prototypes, distances may be comparable and define an overlap between subsets. The distance of an object to each prototype may be such large and its grade of membership to each subset such small that it is considered as isolated. This representation for point defect distributions is quite convenient as it allows deciding if a point defect belongs to a subcascade, to an overlap between subcascades or is isolated. In [27] it is suggested to use CA for associating an ellipsoid to each subcascade K_C and to define a membership function

$$\chi(K_C) = \exp(-\eta^2) \quad \text{with } \eta^2 = \frac{x^2}{\alpha^2} + \frac{y^2}{\beta^2} + \frac{z^2}{\gamma^2}, \tag{3}$$

where η is the Euclidian distance between point defect at (x, y, z) to the cluster centre C, weighted to the cluster size. This definition accounts for the configuration anisotropy and it scales with the cluster size. Points with a grade of membership χ $(K_C) > 1/e$ define the 'core' of K_C.

Up to this point, it is assumed that prototypes exist a priori. In our problem however, the number and the location of subcascades are not known a priori and they must be identified. The Isodata analysis technique is used therefore.

3.3. Isodata analysis

A general presentation is available in [25,26] and we here summarise its application to clouds of point defects. The method consists in building a hierarchy of point defects subsets by iterative splitting of the overall set of vacancies or interstitials. The possibility for a cluster to split is based on a minimal dispersion principle. In [27] an algorithm is described for finding a partition of a cluster into two parts which minimises the sum of their variances projected onto one of its components. This algorithm is used in the present work. In order to decide the status of a point defect, one defines a 'degree of fuzziness' which is used as a parameter, among other in view of comparison with experimental observation which has intrinsically limited resolution. If m is the degree of fuzziness, a point is considered as isolated if

$$\chi(K_C) < 10^{-m} \quad \forall\, K_C. \tag{4}$$

In order to define the overlap between two clusters K and L, one considers the function

$$X = \left| \lg\left(\frac{\chi(K)}{\chi(L)}\right) \right| + 1. \tag{5}$$

X measures the order of magnitude difference between the grade of membership to clusters K and L. This allows to define the degree of fuzziness introduced in (4) by the relation

$$m - 1 < X < m. \tag{6}$$

Points for which this relation is satisfied belong to the overlap between clusters K and L. If $m = 0$ (corresponding to infinite experimental resolution), all points are considered as isolated. If $m = \infty$, they all belong to the same cluster and no splitting is retained. This way, no prototype is defined a priori, but their pattern depends on the degree of fuzziness which has a univocal relation to the resolution of an experimental technique. As a consequence of splitting, grades of membership have to be reassigned and the fuzzy clustering to be repeated iteratively until a stable configuration is found. This iteration procedure includes the possibility of lumping. The separation between subcascades is rejected to the degree m if more than $n^{1/2}$ points of cluster K or L belong to the overlap with the degree of fuzziness m.

The number of points in overlaps is a function of m. It turns out to be no monotonous function of the degree of fuzziness. It has a saw tooth profile and no a-priori rule allows to predict at which value of m the number of points in overlaps will be minimal. However, such a minimum corresponds to the 'hardest' partition of the configuration. In order to find the hardest partition, one uses m as a parameter and seeks for the minimum of a suitable function of m. The hardest partition is the closest to a partition into conventional sets. It is therefore considered as the 'best'. In the case of cascades the function

$$f(m) = N(m)v(m), \tag{7}$$

where $N(m)$ is the number of clusters at degree m and $v(m)$ the fraction of points in overlaps at the same degree, when minimised, efficiently predicts the best partition. It will be used in what follows to characterise the internal structure of point defects in cascades.

At this point, a question of terminology needs to be clarified. In the present study, the concept of 'cluster' introduced above is a set of points having some non-zero distance (according to Eq. (3)) to a prototype. In what follows, the term 'cluster' is used in that sense. This definition is more general than another, often used in describing point defect distributions, where a 'cluster' denotes a set of first, second, or eventually third neighbouring point defects.

4. Displacement cascades structure in Zr

4.1. Overall structure

The overall structure of displacement cascades in Zr is also different from what was found in earlier studies for other materials. In iron for instance [8], cascade volume distributions were found quite widespread and significantly skewed toward large volumes. A well-defined mode was found in these distributions and, because of the long tail toward large volumes, the modal and mean values differ substantially. These volume distributions were evaluated in a PKA energy range where no substantial subcascade formation is expected. Similar distribution profiles were found for cascade anisotropies. The same estimates are here repeated for Zr, in the case of cascades generated by PKA with recoil energies ranging from 5 to 200 keV. Volume distributions associated to vacancies and to interstitials are shown in Fig. 5 for 5 keV and for 50 keV cascades.

In contrast with the case of iron, if one excepts the distribution of volumes associated to interstitials at 5 keV, the modes are in all cases in the first bin of the distributions that display a long tail toward high values. The profiles in Fig. 5 are typical of all distributions obtained at energies above 5 keV.

At all energies, interstitial volume distributions extend to larger values than vacancies, suggesting the usual picture where clouds of vacancies surrounded by interstitials form individual cascades. As shown below, this picture merits some refinement.

The distributions of cascades anisotropies are also quite broad. These are shown in Fig. 6 for a 50 keV PKA energies. Again, the distinction is made between vacancy and interstitial clouds. Fig. 6 is representative of all energies investigated.

4.2. Internal structure

Although the cascade in Fig. 4 can certainly not be considered as representative of all generated cascades, it exemplifies typical features that merit further statistical analysis, now concerning the internal structure. From an overall view of this cascade, it is easily possible to estimate the direction of its principal component and its overall anisotropy. As suggested by the results presented in the preceding section, the vacancy cloud is surrounded by the interstitials. A more detailed look to this cascade suggests it to be partitioned into several subcascades. Within the two-dimensional view available in Fig. 4, five or six subgroups may be distinguished, depending on the criterion used for distinguishing. Each of these

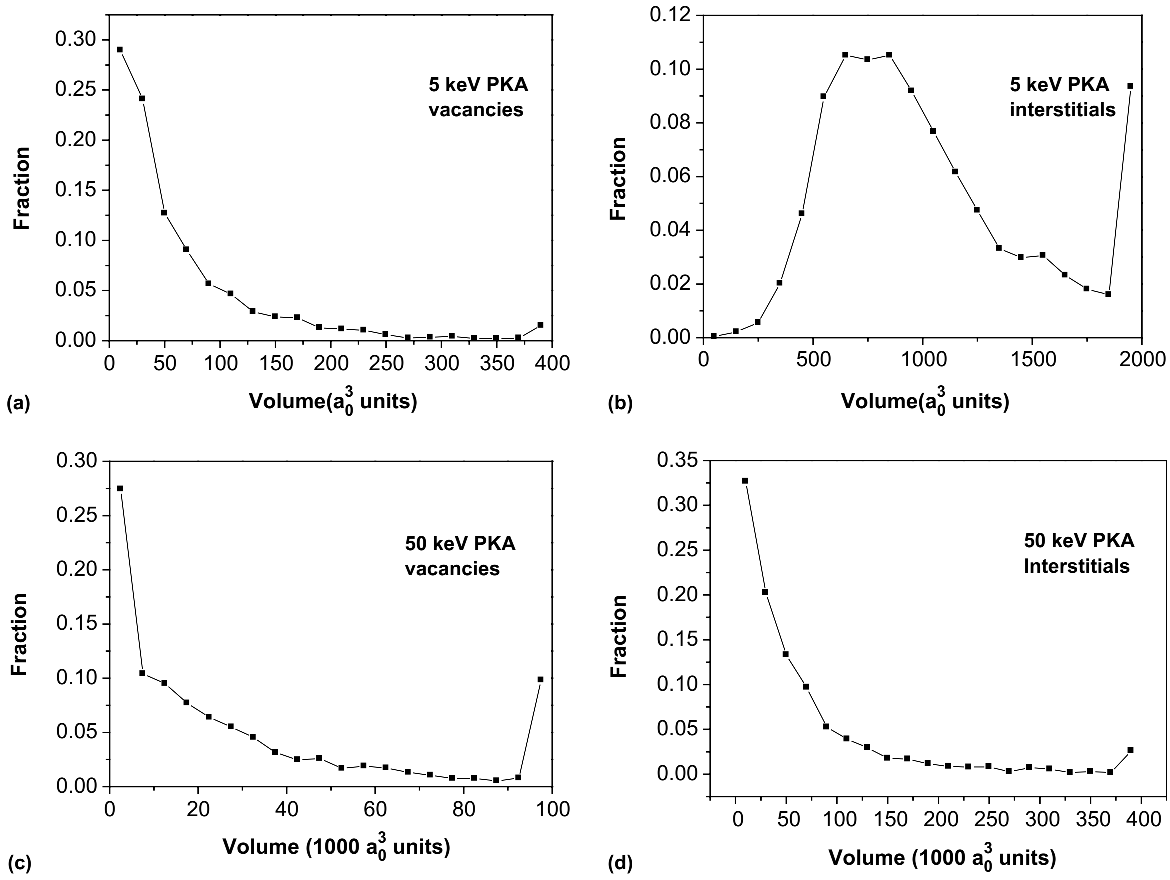

Fig. 5. Volume distributions of the ellipsoids associated to the cascades. The largest volumes are cumulated in the last bin of the distributions. Frequencies are normalised to one cascade.

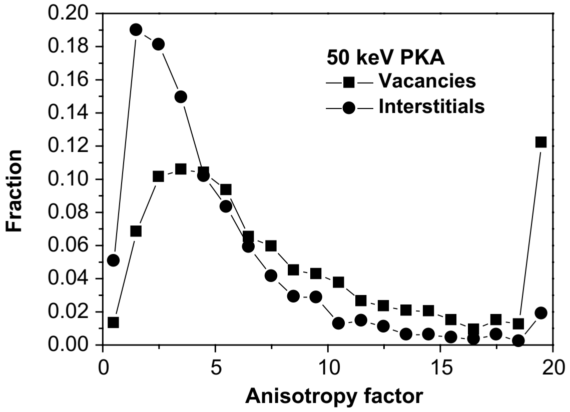

Fig. 6. Distribution of the anisotropy factors of cascades generated by 50 keV PKAs. The anisotropy factor is the ratio between the maximum and minimum elongations of the ellipsoids associated to the cascades. When the anisotropy factor is unity, the cascade morphology is spherical. Results are given for vacancy and interstitial distributions distinctly. The distributions displayed are representative of all distributions obtained with other PKA energies. The largest anisotropies are cumulated in the last bin of the distributions.

groups is seen to be formed by a cloud of vacancies surrounded by interstitials. This cannot be considered as a scaling law because it fails to be correct when looking in still further detail. However, it indicates that cascades and defect clusters in cascades may be self-affine.

We use the fuzzy clustering approach presented in the previous section in order to analyse the clustering into subcascades quantitatively and on a statistical basis. Best clustering configurations are identified. Fig. 7 shows the mean number of best clusters identified as a function of the PKA energy. At high PKA energies, saturation is observed which is probably – and at least partially – due to the limitation of the isodata algorithm of which the splitting hierarchy is not designed to identify more than 16 clusters. The important point to notice in this figure is that the mean number of vacancy clusters identified is systematically larger than the number of interstitial clusters. This suggests that, within one subcascade, more than one group of vacancies can be formed, surrounded by the same cloud of interstitials. Fig. 8 shows the frequency distribution of the number of vacancy (Fig. 8(a)) and interstitial (Fig. 8(b)) clusters identified. This figure illustrates that the distributions become increasingly broader with the PKA energy. It also shows that, if one excepts the lowest PKA energy for which subcascades are exceptional, a significant fraction of cascades do not split into subcascades, and this fraction (40% of interstitial distributions, 30% of vacancy distributions) is not much energy dependent. Therefore, it cannot be considered, as sometimes advocated for other materials, that high-energy cascades are

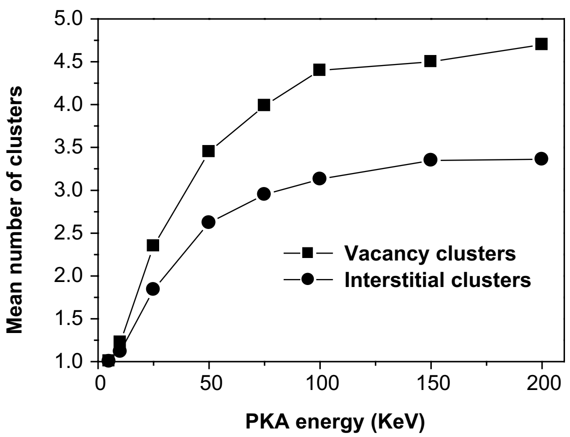

Fig. 7. Mean number of vacancy and interstitial clusters in cascades as a function of the PKA energy. The saturation at high cluster numbers is partly due to the limitation of the isodata algorithm used.

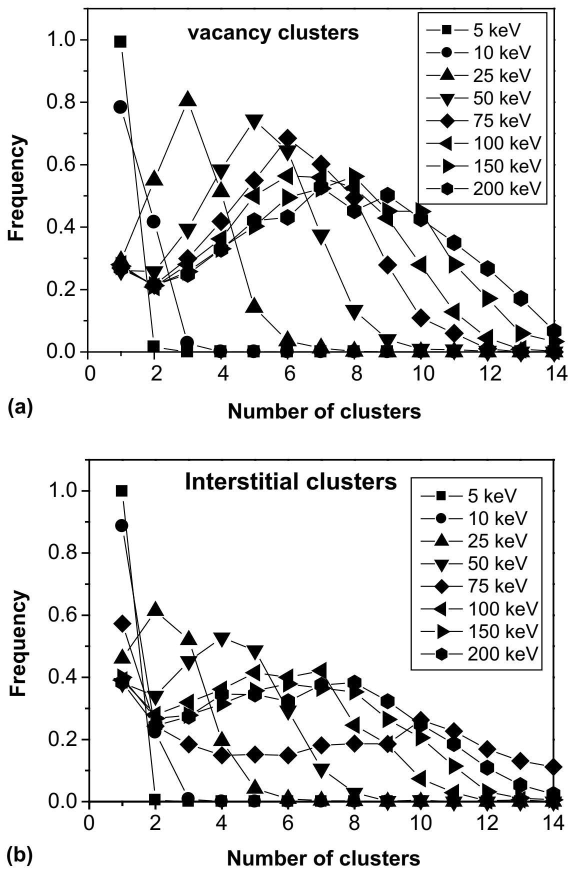

Fig. 8. Frequency distributions of cascades formed by n clusters. The results are displayed for all PKA energies investigated. (a) Vacancy clusters and (b) interstitial clusters.

systematically formed by distinct groups of lower energy cascades.

The spatial extension and anisotropy of each of the clusters identified can be studied, on a statistical basis, the same way as the overall cascades. Therefore, component analysis is thus used, and Fig. 9 gives, with the same scale, the cluster volume distributions for vacancy and interstitial clusters. It is remarkable to notice that the cluster size distributions are almost energy independent. Whatever the PKA energy, a large number of small vacancy clusters is found. However, about half of them form the tail of the distributions. In contrast, as found for the overall cascades and already seen in Fig. 3, interstitial clusters are systematically larger. The anisotropy distributions are shown in Fig. 10. Here again, it is found that the morphology of the clusters in the cascades is not much energy dependent. These results suggest that similar small clusters of vacancies surrounded by interstitials form a high fraction of cascades in Zr. In the average, these small clusters become more numerous and more distant from each other as the energy of the PKA is increased.

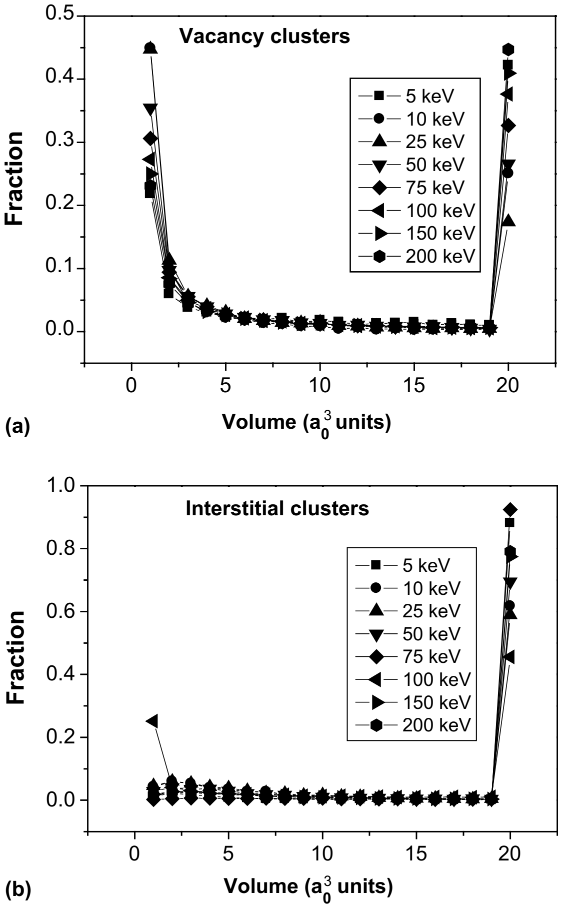

Fig. 9. Distributions of cluster volumes in cascades as obtained for the cases of the different PKA energies considered. (a) Vacancy clusters and (b) interstitial clusters. The largest volumes are reported in the last bin of the distributions. The independence of these distributions on the PKA energy is remarkable.

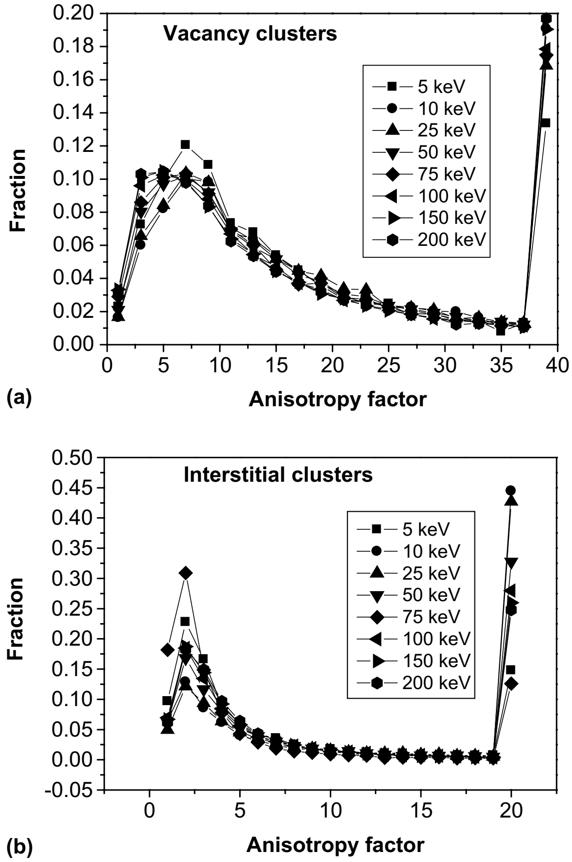

Fig. 10. Distributions of cluster anisotropy factors in cascades as obtained for the cases of the different PKA energies considered. (a) Vacancy clusters and (b) interstitial clusters. The largest anisotropies are reported in the last bin of the distributions. The independence of these distributions on the PKA energy is remarkable.

5. Conclusion

Displacement cascades in Zr display specific features that were not observed in previous studies on cubic materials. These features were also found by repeating several of the calculations described above with different potentials. Because the lattice is hexagonal and atomic separation distances large enough, Frenkel pair distributions have widths more than one order of magnitude broader than in cubic or structureless materials. This is found to correlate with broad PKA range distributions.

This suggests that PKA having long ranges because of their low specific energy loss, produce fewer displacements than those having small ranges. Clusters of vacancies and interstitials are produced and more than one vacancy cluster may be surrounded by the same cloud of interstitials. The width of cluster frequency distributions increases with energy. In contrast, volumes and morphologies distributions are broad and, remarkably, they do not depend on the primary energy. The picture which comes out is that the primaries produce clusters of displacements according to a probability distribution specific to the Zr structure and independent of the PKA energy. The number and separation distances between the small clusters increase with the PKA energy. The net result is overall cascade spatial extents with a mode at the smallest sizes and a tail increasing with the PKA energy.

Beyond what can be predicted in the BCA is the problem of point defect recombination caused by thermal diffusion in the cascade area and the lattice relaxation. The natural technique to tackle this problem is full MD. The dispersion of cascade distributions and the overall spatial extent of cascades are so large that gathering sufficient statistics with large enough simulation boxes may nowadays be unpractical at high PKA energies. The fact that cluster size and morphology distributions are energy invariant contributes to save the situation.

Acknowledgment

This work is supported by the European Communities under contract FIKS-CT-2001-00137.

References

[1] M. Griffiths, J. Nucl. Mater. 159 (1988) 190.
[2] Thematic European research project 'Simulation of Radiation Effects in Zr–Nb Alloys: applications to stress corrosion cracking behaviour of iodine-rich environment'.
[3] M. Griffiths, R.C. Styles, C.H. Woo, F. Phillipp, W. Frank, J. Nucl. Mater. 208 (1994) 324.
[4] C.H. Woo, J. Nucl. Mater. 276 (2000) 90.
[5] W.G. Eckstein, Computer Simulation of Ion-Solid InteractionsSpringer Series in Materials Science, vol. 10, Springer-Verlag, Berlin, 1991.
[6] M.T. Robinson, in: R. Behrisch (Ed.), Sputtering by Particle Bombardment, vol. 1, Springer-Verlag, Berlin, 1991.
[7] M. Hou, Z.Y. Pan, Radiat. Eff. Def. Sol. 142 (1997) 941.
[8] A. Souidi, M. Hou, C.S. Becquart, C. Domain, J. Nucl. Mater. 295 (2001) 179.
[9] M. Hou, A. Souidi, C.S. Becquart, Nucl. Instrum. and Meth. B 196 (2002) 31.
[10] M. Hou, Nucl. Instrum. and Meth. B 187 (2002) 20.
[11] M.T. Robinson, Phys. Rev. B 40 (1989) 10717.
[12] G. Molière, Z. Naturforsch. A 2 (1947) 133.
[13] O.B. Firsov, Zh. Eksp. Teor. Fiz. 33 (1957) 696;
O.B. Firsov, Sov. Phys. JETP 6 (1958) 534.
[14] D.J. Bacon, A.F. Calder, F. Gao, Radiat. Eff. Def. Sol. 141 (1997) 283.
[15] R. Stoller, J. Nucl. Mater. 276 (2000) 22;
R.E. Stoller, L.R. Greenwood, in: S.T. Rosinski, M.L. Grossbeck, T.R. Allen, A.S. Kumar (Eds.), Effects of Radiation on Materials, ASTM STP 1405, American Society of Testing and Materials, West Conshohocken, PA, 2001, p. 204.
[16] L. Malerba, D. Terentjev, P. Olsson, R. Chakarova, J. Wallenius, J. Nucl. Mater. 329–333 (2004) 1156.
[17] G. Kinchin, R. Pease, Rep. Prog. Phys. 18 (1955) 1.
[18] M.J. Norgett, M.T. Robinson, I.M. Torrens, Nucl. Eng. Des. 33 (1975) 50.
[19] F. Gao, D.J. Bacon, L.M. Howe, C.B. So, J. Nucl. Mater. 294 (2001) 288.
[20] R. Stoller, A.F. Calder, J. Nucl. Mater. 283–287 (2000) 746.
[21] M.T. Robinson, I. Torrens, Phys. Rev. B 9 (1974) 5008.
[22] G. Leibfried, Bestrahlungseffekte in Festkörpern, Teubner, Stuttgart, 1965.
[23] J. Lindhard, M. Scharff, H.E. Schiott, Mat. Fys. Medd. Dan. Vid. Selsk. 33 (1963) 14.
[24] L.A. Zadeh, Inf. Control 8 (1965) 338.
[25] E.H. Ruspini, Thesis, University of California, 1977, unpublished.
[26] A. Kandel, Fuzzy techniques in pattern recognition, Wiley, New York, 1982.
[27] M. Hou, Phys. Rev. A 39 (1989) 2817.
[28] M. Hou, Phys. Rev. B 31 (1985) 4178.